Published in final edited form as:
Anal Chem. 2009 December 1; 81(23): 9657–9663. doi:10.1021/ac901789w.

Advantages and Artifacts of Higher Order Modes in Nanoparticle Enhanced Back-Scattering Raman Imaging

Zachary D. Schultz[1], **Stephan J. Stranick**[2], and **Ira W. Levin**
Laboratory of Chemical Physics, National Institute of Diabetes and Digestive and Kidney Diseases, National Institutes of Health, 9000 Rockville Pike, Bethesda, MD, 20892

Zachary D. Schultz: ; Stephan J. Stranick: ; Ira W. Levin: iwl@helix.nih.gov

Abstract

In order to facilitate nanoparticle enhanced Raman imaging of complicated biological specimens, we have examined the use of higher order modes with radial and azimuthal polarizations focused onto a Au nanoparticle AFM tip utilizing a back-scattering reflection configuration. When comparing the Raman intensity profiles with the observed sample topography, the radial polarized configuration demonstrates enhanced spatial resolution. This enhanced resolution results from the direction of the induced electron oscillation in the metal nanoparticle oriented by the electromagnetic field at the laser focus. The electric field component along the direction of laser propagation, attendant to the radial polarization, creates an enhanced field along the z-axis and normal to the sample. Substantial enhancement is observed utilizing an intermediate numerical aperture objective (NA = 0.7), necessary for back-scattering measurements. The azimuthal polarization, similar to linear polarization, results in an enhanced field predominantly parallel to the sample, resulting in imaging artifacts. The Raman intensity profiles observed as the exciting laser polarization is switched between either a radially polarized or an azimuthally polarized state illustrate these imaging artifacts. Because azimuthal polarization arises readily from changes in the incident polarization onto the mode converter, the results presented here aid in identifying such artifacts when analyzing nanoparticle enhanced Raman spectroscopic images. Due to the power law decay of the enhanced field, an enhancement orientation normal to the sample enables contrast between structures smaller than the tip dimensions as the apex of the nanoparticle tip, where the enhancement is strongest, passes over the sample. These effects are demonstrated using both carbon nanotube and fixed biological samples.

Introduction

Raman spectroscopic imaging has long provided a non-destructive spectroscopic means of obtaining chemical information about molecular species through the inelastic scattering of monochromatic light at spectral frequencies corresponding to vibrational modes.[1-5] Since inelastic scattering processes are highly inefficient, the resulting low signal to noise levels necessitate long acquisition times, which limit sensitivity. The discovery that a metal surface gives rise to significant enhancements in Raman scattering[6] increased the sensitivity to near single molecule detection[7, 8] and has led to significant efforts in understanding its origins.[9] While some experiments indicate that “hotspots” give rise to extremely large spectral enhancements,[10] it is accepted that the electromagnetic field is enhanced at the surface of metallic nanostructures by means of a coupling to localized surface plasmons. This

Correspondence to: Ira W. Levin, iwl@helix.nih.gov.

[1]Current Address: Department of Chemistry and Biochemistry, University of Notre Dame, 251 Nieuwland Science Hall, Notre Dame IN 46556-5670

[2]Surface and Microanalysis Science Division, National Institute of Standards and Technology, 100 Bureau Dr., Gaithersburg, MD, 20899

understanding has given rise to numerous applications involving the Raman enhancements accompanying metal nanostructures.[9, 11-13]

The use of a metal nanostructure with a scanning probe microscope (SPM), referred to as tip enhanced Raman scattering (TERS) or apertureless near-field microscopy, provides an approach toward using this enhanced Raman signal to spatially resolve molecular components.[12-15] Since the first demonstration of TERS,[16] this method has provided high sensitivity molecular detection via Raman scattering.[14, 17-20] Examples of applications that have been studied by TERS include detection of nucleotides,[19] inspection of silicon strain,[21, 22] examination of carbon nanotubes,[23-26] and inspection of biofilms.[27] This increased sensitivity has enabled nanometer spatial resolution imaging.[28, 29] In one example, utilizing TERS in ultra high vacuum, a single dye molecule was imaged.[30] Another recent report suggests that sub-nanometer spatial resolution Raman imaging may be possible.[29]

The localized surface plasmon that gives rise to the enhanced electromagnetic field originates from a light induced oscillation of conduction band electrons within metal nanostructures,[9, 11] with the frequency dependence of the induced oscillation being related to the metal identity, size and shape of the nanostructure.[9, 11] The polarization of the exciting laser beam, important for optimizing the Raman enhancment,[31-33] insures efficient coupling of the electromagetic field to the localized plasmon mode. For elongated metal coated SPM tips, the electromagnetic field requires a component along the long axis of the tip.[34] This has been accomplished using both side illumination with linearly polarized light,[13, 35, 36] and radial laser polarization.[37, 38]39 The use of a high numerical aperture optic, such as an oil immersion objective, results in formation of a predominantly longitudinal mode oriented between the SPM tip and the sample. However, for opaque samples this requires a custom-designed optic, such as the parabolic mirror with an SPM tip passing through the center utilized by Steidtner and Pettinger.[39] Side-illumination provides another approach capable of probing opaque samples, but alignment of the laser with the tip and tip-shadowing effects have been reported to be problematic.[22] Back-scattering, or reflective, geometries have not been largely investigated with radial polarization due to the lower numerical aperture associated with long working distance objectives. AFM probes that provide unobstructed access from above make TERS backscattering measurements possible and readily accomplished through an upright microscope. The incorporation of TERS into a traditional upright microscope offers the advantage of initial macroscale screening followed by nanoscale investigation of a region of interest on any sample accessible by traditional micro-spectroscopy; however, previously reported enhancements obtained in a backscattering geometry were not competitive with enhancements observed in other configurations.

In the case of spherical nanoparticles, either free standing or attached to atomic force microscope (AFM) tips, the polarization of the exciting radiation influences the direction of the induced oscillation and thus the directionality of the enhanced electromagnetic field. Traditional Raman polarization analyses take advantage of the unidirectional electric field at the focus of the linearly polarized light and the resulting polarization in the Raman scattered photons. Interestingly, polarization filtering, analogous to classic Raman polarization measurements, is reported to be an effective method of distinguishing the near-field scattering from the far-field background signal.[22] However, the Hermite-Gaussian modes associated with radial and azimuthally polarized light possess different electric field intensity distributions when focused, in comparison to that of linearly polarized light.[40] The focal field distributions of radial and azimuthal polarized beams were recently demonstrated to measure the x, y, and z Raman tensor components from crystalline α-quartz.[41] The numerical aperture (NA) of the focusing optic modulates the proportions of field intensity in the x, y, and z directions at the laser focus. At low NA, the electric field of a radially polarized beam orients predominantly in a lateral (x or y) direction. As the NA of the focusing optic increases, so does the proportion

of the electric field that orients in the z direction.[40, 41] It is worth noting, that a small, non-zero, z-component has been observed at very low NA, but increases substantially at higher NA.[40] The results presented in the present study illustrate the manner in which radial and azimuthal polarizations influence both the magnitude of the enhancement and also the directionality of the enhanced field that affects the spatial resolution obtained in backscattering TERS imaging experiments. Radial polarization is shown to be beneficial for imaging; however, because an azimuthal polarization is readily generated from a polarization change of the laser onto the mode converter, the results presented here identify imaging artifacts that can arise from the azimuthal state. The use of intermediate NA objective is shown to produce substantial contrast enabling opaque samples, relevant in both material science and biological applications, to be readily examined in a TERS system established around an upright microscope.

Experimental

The tip enhanced Raman microscope instrument is a customized version of a combined AFM-Raman system comprised of a Nanonics Multiview 2000 AFM and a Renishaw InVia Raman microscope and is based on the reflective geometry originally reported by Sun and Shen.[42, 43] The Multiview 2000 AFM was mounted on a Prior Proscan II mechanical stage and used in phase feedback to provide non-perturbative topographical measurements. The AFM was equipped with a Au chemical mechanical polished (CMP) nanoparticle TERS tips (Nanonics Supertips, LTD.) with a reported nanoparticle diameter < 200nm. Laser excitation was provided by a Melles-Griot Krypton ion laser emitting up to 200 mW (CW) at 647.1 nm and was coupled to the Raman microscope by a single mode fiber. Typically, the laser intensity was attenuated to provide 1-2 mW at the sample. A schematic of the optical path used is illustrated in figure 1. The laser intensity from the single mode fiber is collimated and polarized in the vertical direction before passing into the InVia microscope. The laser spot size is adjusted using the beam expansion optics of the InVia microscope to a size of 6mm, which is incident on a transmissive liquid crystal mode converter (ArcOptix, S.A.), consisting of a phase retarder to correct for phase distortion, a polarization rotator, and the theta-cell that generates the converted polarization. Depending upon the incident polarization of laser beam, the light passing through the mode coverter is transformed into either a radially polarized or an azimuthally polarized beam. The polarization rotator of the mode converter allows the incident polarization to be rotated 90° by applying an external voltage, enabling straightforward conversion between the radial or azimuthal polarizations. The converted laser polarization is passed to an upright microscope, where the laser radiation is focused into a diffraction-limited spot on the AFM sample. A Nikon L Plan SLWD 100× objective, with an NA = 0.70 and a working distance of 6.5 mm, is used to both focus the laser light onto the sample and to collect the resultant Raman scattering. The TERS nanoparticle tip is positioned within the laser focus to provide the highest near-field Raman enhancement. The Stokes-shifted Raman scattering is separated from the Rayleigh scattering by means of an edge filter. The Raman signal is dispersed on a 1200 grooves/mm grating and collected on a CCD camera.

Samples were prepared by depositing analytes onto Au coated silicon substrates prepared by thermal evaporation of 200 nm Au onto a 1 nm Cr adhesion layer on a Si(100) wafer. Single wall carbon nanotubes (CNT), prepared by the high pressure CO method, were dispersed in benzene. Substrates were immersed in the CNT-benzene solution and then allowed to dry. Benzene is a hazardous solvent and should be handled in chemical hood utilizing the proper personal protective equipment. Rod photoreceptor cells, isolated from bull frogs (*rana catesbiana*), were fixed in 2.5% glutaldehyde solution. Fixed rod cells were deposited onto the Au coated Silicon substrates directly from the fixation solution and allowed to dry prior to measurement.

AFM data analysis was performed using WSxM 4.0 Develop 10.1. Raman and TERS images were processed using algorithms in ENVI 4.5 + IDL 7.0 (ITT Visual Information Solutions).

Results and Discussion

Figure 2 shows the tip enhanced Raman signal obtained from a CNT sample using a radially polarized and an azimuthally polarized laser beam, as well as the far field Raman signal observed when the nanoparticle tip is retracted from the surface. Consistent with previous reports,[37, 38, 44] the radially polarized laser beam shows the greatest enhancement. The magnitude of the enhancement observed here is substantially larger than that in our previous experiments.[44] The origin of the increased enhancement is two fold. First, in the present study, an NA = 0.7 objective is used, compared to an NA = 0.45 objective in the previous work. The increased NA objective results in a tighter laser focus, increasing the magnitude of the electric field that is enhanced by the nanoparticle tip. The increased NA results in increased tip enhanced scattering in both polarization states. Second, the radial polarization is observed to result in a substantial increase in tip enhanced Raman scattering compared with the scattering from the azimuthal polarization. This second enhancement arises from the increased z-polarization attendant to a higher numerical aperture objective.[40, 41] The electric field focal field distribution induces the plasmon oscillation in the metal nanoparticle in the direction of the electric field component at the focus, resulting in an enhanced electromagnetic fields along specific nanoparticle surfaces.[9] The enhancement from the nanoparticle results in significant increase in scattering in the immediate vicinity of the probe offering both increased sensitivity and higher spatial resolution contrast. For a nanoparticle in the radially polarized laser focus, a significant portion of the enhanced field forms along the top and bottom of the nanoparticle, increasing the interaction between the CNT sample and the nanoparticle tip and giving rise to the enhancement in the TERS spectrum. For the azimuthally polarized beam, the enhanced field forms predominantly in the lateral, x-y direction, resulting in a stronger electromagnetic field enhancement along the sides of the nanoparticle. Enhancement is still observed under these conditions, but the consequences of this for imaging are worth further investigation. The enhancement observed in figure 2 is comparable to that reported by physically manipulating a Au nanoparticle into close proximity with carbon nanotubes. [45]

For samples, with topographical features of similar size to the nanoparticle tip, the directionality of the electric field can exhibit interesting results in TERS images. In Figure 3A, the AFM topographical image of carbon nanotubes dispersed onto a substrate is shown. The large bundle of carbon nanotubes in the center of the image displays a small valley in the linear profile obtained along the diagonal, as shown in Figure 3B. The distance measured from the first topographical peak at 3.21 μm to the rising slope of the second peak at 3.51 μm is close to the dimensions of the nanoparticles tip (~200 nm). In the case of samples with topography such as this, the directionality of the electric field enhancement becomes important.

Figure 4 shows the TERS results along the same line delineated in Figure 3B. Figure 4A plots the Raman spectra from the carbon nanotubes obtained using radial polarization in the range from 1200 – 1700 cm^{-1} against distance along the line from the AFM scan. The G-band (1590 cm^{-1}) and D-band (1310 cm^{-1}) transitions of the carbon nanotubes are clearly visible. Tracing the Raman intensity, of the G-band transition, one obtains the profile shown in Figure 4B. The Raman intensity profile shows a close similarity to the AFM topography observed along this line. In particular, the two maxima observed in the AFM are also observed in the TERS measurement. It is worth noting that the dimensions of these spatial features are below the diffraction limit, which are not resolvable without the near-field enhancement from the nanoparticle tip. Raman spectra obtained using the azimuthally polarized laser beam are plotted in Figure 4C over the same frequency range along the same diagonal profile in the AFM scan. The same vibrational features, the D-band and G-band transitions, are observed in the Raman

spectrum; however, upon examining the Raman intensity profile of the G-band (Figure 4D), the minima observed in the AFM scan is no longer observed. Instead, a maximum is observed in the Raman profile for the region that is known to be a valley from the AFM topography. AFM scans performed before, during, and after the TERS measurement confirm the continued existence of the valley, indicating that no tip induced change in topography occurred. The magnitude of the observed Raman signal indicates that enhancement is occurring from the nanoparticle tip.

The origins and consequences of the polarization on the observed Raman Intensity profile are important for analytical microscopy and spectroscopy using plasmon enhancements motifs. It has been recognized that polarization plays an important role in generating enhancements along scanning probe tips for near-field excitation.[13] The principal concern, regarding polarization, was to align the electric field with the elongated axis of the tip, to generate the greatest enhancement. In our case, utilizing a spherical nanoparticle, such concerns might appear trivial; however, our results indicate that polarization still plays an important role in determining the spatial properties of the enhanced field. Since the enhancement in the electric field results from the induced oscillation of electrons in metallic nanostructures,[9] the direction of electric field oscillation associated with the laser polarization is expected to influence the directionality of the enhanced field. The spatial resolution for a spherical nanoparticle tip is then the convolution of the tip dimensions with the effective enhanced electric field. Thus, the spatial relationship between a nanoparticle AFM tip and an analyte can have a pronounced impact on the near field enhancement. Using radial polarization, the field is significantly enhanced in the direction of propagating laser beam, effectively enhancing the Raman scattering specifically beneath the nanoparticle tip. In the case of the azimuthally polarized beam, the electric field is enhanced normal to the laser beam direction of propagation, generating an increased enhancement along the sides of the nanoparticle tip. In the case where an analyte shows a valley with dimensions approaching the dimensions of the tip, an artifactual peak is observed in the Raman intensity profile, such as that seen in Figure 4D. In situations where the sample is enhanced on only 1 side of the nanoparticle tip, this effect would generate a small spatial offset. In the Raman results shown above, this offset is less than the distance between points, making it less obvious. The Raman intensity observed for the azimuthal polarization at 3.25 μm in Figure 4 is greater than that for the radial polarization because the sample topography matches the shape of the nanoparticle tip, which effectively doubles the sample concentration experiencing the electromagnetic field enhancement along the sides of the nanoparticle; thus, producing a misleading intensity in the Raman intensity profile. By examining the Raman intensities in a relatively flat region, such as that near 7 μm in Figure 4, the radial polarization reliably evinces a larger enhancement arising from the increased enhancement on the bottom of the nanoparticle. Previous studies utilizing nanoparticle tips have exhibited interesting spatial intensity profiles, showing Raman intensity maxima to the sides of the object, opposed to a centroid as a nanoparticle tip passes over the object of interest. [46] This effect arises from the lateral oscillation induced in the nanoparticle by the linearly polarized laser excitation. This artifact can be corrected using radial polarization. The relative electric field strengths of the z-polarized versus the in-plane polarization at the focus of a radially polarized beam are known to correspond to the focusing angle of the laser beam. [40] Since focusing angle increases with numerical aperture, high numerical aperture objectives are used to generate electromagnetic fields oriented in predominantly the z-direction. [38, 39, 41] The intermediate NA objective (NA=0.7) creates an enhanced, nearly uniform field distributed, for instance, in the x-z plane. The increased electric field strength in the z-direction corrects the Raman intensity profile by showing maximum enhancement as the tip moves over the structure, compared to having maximum enhancement to the sides generating increased Raman intensities as the tip approaches and then passes by the structure. Caution should be observed when the Raman intensity indicates maxima offset from the known topography. A change in laser polarization could result in increased azimuthal character, creating imaging artifacts. Because the surface

enhancement of the electric field is known to decay at a length proportional to the radius of curvature, in the case where the polarization generates the enhanced electromagnetic field along the direction of tip scanning, the effective spatial resolution is decreased. The radial polarization effectively redistributes the electromagnetic intensity, increasing the enhancement below the nanoparticle tip, maintaining the spatial resolution associated with the tip geometry and the correlation with the measured AFM topography.

It has been shown that polarization plays a role in generating the enhancement in other plasmonic structures. Nano-structured substrates exhibit changes in enhancement dependent upon the incident polarization, where the polarization is related to the coupling between adjacent nanoparticles.[47] An interesting observation is that using azimuthally polarized light, the intensity is shifted into the x-y plane. By rotating the polarization of the laser incident on the LC mode converter (Fig. 1) by 90°, one can control whether the nanoparticle is preferentially enhancing above and below or side-to-side. The principle difference between the azimuthal polarization and linear polarization is linear polarization oscillates in either x or y, azimuthal polarization induces oscillations in both x and y. This further supports that by changing the NA of the objective and the incident polarization of the laser onto the mode converter, the proportions or shape of the enhancing electromagnetic field can be controlled.[41] For a metal nanoparticle bound to a substrate of interest, higher order mode polarization states may offer a means of probing in a lateral vs. normal direction to the nanoparticle.

The vibrational modes observed in Figure 4 illustrate that the TERS image can resolve the location of carbon nanotubes. For analytical purposes, being able to resolve sub-components of a heterogeneous sample is also important. The ability to obtain chemical information from the associated vibrational spectrum is a key benefit of spectroscopic imaging. Figure 5 is an example of analytical microscopy for distinguishing sub-components within a heterogeneous mixture using radial polarization. Figure 5A shows the Raman spectra obtained along the same diagonal depicted in Figure 3, but in the frequency range (100-600 cm^{-1}) covering the radial breathing modes of the carbon nanotubes. Although several modes corresponding to different nanotube diameters are observed in this range, the Raman intensity profiles for the modes at 196 and 283 cm^{-1} are illustrated in Figure 5B. Specifically, the Raman shift frequencies of the radial breathing modes are related to the diameters of the single walled carbon nanotube.[48] The profiles shown in figure 5B correspond to nanotubes with approximate diameters of 12 and 8 Å, respectively. Interestingly, the bundle of tubes that gives rise to the large topographical feature appears to consist predominantly of 8 Å nanotubes. The feature observed between 6-7 μm in the diagonal profile shows a much stronger signal from the 12 Å nanotubes, supporting heterogeneous distributions of nanotubes and not a simple difference in Raman polarizability. Figure 5 clearly demonstrates that the spectra obtained in TERS imaging, utilizing large nanoparticles, can be used to identify chemical compositions at the nanoscale.

The spatial resolution demonstrated in these results is proportional to the dimensions of the nanoparticle AFM tip used. Examination of topographic features in the AFM image indicates a 190 nm diameter tip, consistent with the manufacturer's specification. Large nanoparticles, such as these, have not been used extensively in TERS microscopy. Smaller nanostructures offer increased spatial resolution, consistent with tip dimension limited resolution, and have been utilized in other reports.[12, 13] It is important to consider the power dependence of electromagnetic field enhanced at the nanoparticle surface. The Intensity of a vibrational mode enhanced by the field generated at the nanoparticle surface decays according the relation:

$$I_{\text{Enhancement}} = \left(\frac{r_{\text{nanoparticle}} + d}{r_{\text{nanoparticle}}} \right)^{-10}$$

Equation 1

where r is the nanoparticle radius of curvature and d is the distance from the nanoparticle surface.[9] The consequence of equation 1 is that for small nanoparticles, less than 10 nm diameter, the electric field enhancement extends only to those molecules at the nanoparticle surface. For a 10 nm particle, greater than 95% of the enhanced field has decayed 2 nm from the surface. For analysis of small molecule adsorbates, this is sufficient. In the case of macromolecular assemblies, a greater working distance from the nanoparticle is desirable. In the case of 200 nm nanoparticle tips utilized in these experiments, 50% of the enhanced electromagnetic field persists at 7 nm from the surface and 25% of the enhancement persists at a distance of 15 nm from the surface. The 95% decay point for our 200 nm nanoparticle is found ca. 35 nm from the nanoparticle surface. In the presence of lateral electromagnetic fields, such as at the focus of the azimuthally polarized beam, the spatial resolution is diminished by this factor. In figure 3B, the size of the valley at 3.5 μm is approximately 300 nm. When we add this enhancement distance to the tip dimensions for the azimuthally polarized beam, it is clear that near the bottom of the valley the azimuthal polarization enhances the carbon nanotubes on both sides, creating the artifactual peak in the Raman intensity profile (Fig. 4D). For the radially polarized beam, in which the electromagnetic field is directed into the sample, a measure of penetration depth arises, but does not appear to diminish the lateral resolution.

The absolute enhancement observed here is greatly improved, relative to other back scattering reports, but is still less than other TERS experiments. The advantage of this approach is the broad applicability. By using an upright microscope, large samples can be surveyed for spots of interest and then examined with increased molecular sensitivity and improved spatial contrast. The incident laser is unobstructed enabling investigation of a large diversity of samples.

A cellular membrane, for which the lipid bilayer is approximately 10-20 nm thick, plus an additional thickness to account for proteins and carbohydrates, represents an example of a macromolecular assembly with dimensions that benefit from the TERS approach described above. Figure 6 shows the visible image of a fixed rod photoreceptor cell (Fig. 6A) and the Raman TERS map (Fig. 6B) generated from the vibrational mode observed at 1655 cm^{-1} (Fig. 6C) obtained from 2.5 μm × 2.5 μm square outlined on the visible image. In this case a visible image of large cell, selected from numerous cells collected on a substrate, was surveyed and then a section of the outer membrane examined in more detail. The peak in the Raman spectrum at 1655 cm^{-1} is commonly associated with Amide I vibrational mode. Changes in the frequency of this mode have been associated with protein secondary structure; namely, Raman spectral peaks for an α-helix, β-sheet, and random coil are observed at 1652-1662, 1672-1674, and 1665-1668 cm^{-1}, respectively.[49] The variations in peak intensity observe in the Raman map suggest variations in secondary structure of membrane-associated proteins in the plasma membrane. Polyunsaturated lipid acyl chains also exhibit vibrations in this region, although, the fixation process oxidizes these unsaturated bonds.

Figure 6B illustrates Raman pixel spacings of 97 nm. Interestingly, we note a variation in the Amide I vibrational mode intensities of approximately half the diameter of the tip. Because of the power dependence of the surface plasmon enhancement in the nanoparticle tip, this suggests that the enhancement is only strong enough to be observed as the apex of the nanoparticle passes over the molecular analyte, in this case a particular protein secondary structure. The sensitivity of our experiment suggests that the observed enhancements arise from multiple helical sub-units; however, future optimization of the experiment may enable single sub-unit detection. Currently, similar to other super-resolution fluorescence imaging techniques, such as PALM and STORM microscopy,[50, 51] this intensity variation provides a statistical means of locating the position of molecular species below the tip-limited resolution.[29] In our experiment the resolution limit is smaller than the tip dimensions, but still coupled to the curvature that controls the change in the enhanced field with distance. This concept has been

previously suggested as a means of using TERS for sequencing nucleic acid strands.[52] In these cases, the directionality of the electromagnetic enhancement is critical, such that the molecule experiences the greatest enhanced field at the apex of the nanostructure tip. The radial polarized laser beam in our experiments increases the magnitude at the bottom of the particle, and is thus critical for obtaining this increased contrast.

These results indicate the potential for TERS imaging to provide insights in molecular distributions, on the nanoscale, associated, for example with diseased states. Large cell arrays, such as those commonly used in histopathological analysis,[53] can be scanned on the macro-scale and areas of interest can then be analyzed with more detail. While the current Raman imaging is a slow process, requiring 5-30 s per pixel for cellular samples, this analysis is still appropriate for other fixed biological samples, such as those used in histopathology or those used in cryo-electron microscopy. In these preserved samples, the Raman nanoscale imaging offers a non-destructive method of investigating molecular distributions.

Conclusions

The results presented here illustrate the advantages of radially polarized laser excitation on the directionality of the Raman enhancement in nanoparticle imaging applications. The use of an intermediate NA objective is demonstrated to produce a substantial increase in the near-field scattering associated with radial polarized illumination. In the reflective geometry, utitilizing a nanoparticle SPM tip, radial laser polarization effectively orients the enhanced electromagnetic field along the tops and bottoms of the nanoparticle surfaces. This provides for superior spatial contrast by correcting the direction of the enhancement relative to the nanoparticle shape. Artifactual signals arising from azimuthally polarized light are illustrated to raise awareness when analyzing TERS images obtained using higher order modes. Radial polarization, also allows a TERS capability of spatial resolution below the dimensions of the tip. By improving the magnitude of the near-field signal in a back-scattering configuration, this experimental methodology shows potential for elucidating biological structures at nanoscale levels. The polarization effects observed are also relevant when using nanoparticles for other, non-TERS, Raman detection applications.

Acknowledgments

The authors thank Shuko Yoshikami for assistance isolating rod photoreceptor cells. This work was funded through the NIDDK intramural research program. ZDS acknowledges support from NIH K99RR024367.

References

1. Chourpa I, Lei FH, Dubois P, Manfait M, Sockalingum GD. Chemical Society Reviews 2008;37:993–1000. [PubMed: 18443684]
2. Navratil M, Mabbott GA, Arriaga EA. Analytical Chemistry 2006;78:4005–4019. [PubMed: 16771538]
3. Levin IW, Bhargava R. Annual Review of Physical Chemistry 2005;56:429–474.
4. Pappas D, Smith BW, Winefordner JD. Applied Spectroscopy Reviews 2000;35:1–23.
5. Treado PJ, Morris MD. Applied Spectroscopy Reviews 1994;29:1–38.
6. Fleischmann M, Hendra PJ, McQuillan AJ. Chemical Physics Letters 1974;26:163–166.
7. Kneipp K, Wang Y, Dasari RR, Feld MS. Applied Spectroscopy 1995;49:780–784.
8. Nie S, Emory SR. Science 1997;275:1102–1106. [PubMed: 9027306]
9. Stiles PL, Dieringer JA, Shah NC, Van Duyne RP. Annual Review of Analytical Chemistry 2008;1:601–626.
10. Fang Y, Seong NH, Dlott DD. Science 2008;321:388–392. [PubMed: 18583578]
11. Love SA, Marquis BJ, Haynes CL. Applied Spectroscopy 2008;62:346A–362A.

12. Verma P, Inouye Y, Kawata S. Surface-Enhanced Raman Scattering: Physics and Applications 2006;103:241–260.
13. Pettinger B. Surface-Enhanced Raman Scattering: Physics and Applications 2006;103:217–240.
14. Novotny L, Stranick SJ. Annual Review of Physical Chemistry 2006;57:303–331.
15. Drezet A, Hohenau A, Krenn JR, Brun M, Huant S. Micron Microscopy of Nanostructures 2007;38:427–437.
16. Stockle RM, Suh YD, Deckert V, Zenobi R. Chemical Physics Letters 2000;318:131–136.
17. Domke KF, Zhang D, Pettinger B. Journal of the American Chemical Society 2007;129:6708–+. [PubMed: 17480079]
18. Domke KF, Zhang D, Pettinger B. Journal of the American Chemical Society 2006;128:14721–14727. [PubMed: 17090060]
19. Rasmussen A, Deckert V. Journal of Raman Spectroscopy 2006;37:311–317.
20. Saito Y, Motohashi M, Hayazawa N, Iyoki M, Kawata S. Applied Physics Letters 2006;88
21. Hayazawa N, Motohashi M, Saito Y, Ishitobi H, Ono A, Ichimura T, Verma P, Kawata S. Journal of Raman Spectroscopy 2007;38:684–696.
22. Lee N, Hartschuh RD, Mehtani D, Kisliuk A, Maguire JF, Green M, Foster MD, Sokolov AP. Journal of Raman Spectroscopy 2007;38:789–796.
23. Hartschuh A, Sanchez EJ, Xie XS, Novotny L. Physical Review Letters 2003;90
24. Yano T, Verma P, Kawata S, Inouye Y. Applied Physics Letters 2006;88
25. Hayazawa N, Yano T, Watanabe H, Inouye Y, Kawata S. Chemical Physics Letters 2003;376:174–180.
26. Hartschuh A, Qian H, Meixner AJ, Anderson N, Novotny L. Surface and Interface Analysis 2006;38:1472–1480.
27. Schmid T, Messmer A, Yeo BS, Zhang WH, Zenobi R. Analytical and Bioanalytical Chemistry 2008;391:1907–1916. [PubMed: 18427785]
28. Gerton JM, Wade LA, Lessard GA, Ma Z, Quake SR. Physical Review Letters 2004;93
29. Ichimura T, Fujii S, Verma P, Yano T, Inouye Y, Kawata S. Physical Review Letters 2009;102:186101–186104. [PubMed: 19518888]
30. Steidtner J, Pettinger B. Physical Review Letters 2008;100
31. Itoh T, Hashimoto K, Ozaki Y. Applied Physics Letters 2003;83:2274–2276.
32. Grand J, de la Chapelle ML, Bijeon JL, Adam PM, Vial A, Royer P. Physical Review B (Condensed Matter and Materials Physics) 2005;72:033407–033404.
33. Hongxing Xu MK. ChemPhysChem 2003;4:1001–1005. [PubMed: 14562448]
34. Picardi G, Nguyen Q, Ossikovski R, Schreiber J. Applied Spectroscopy 2007;61:1301–1305. [PubMed: 18198021]
35. Pettinger B, Ren B, Picardi G, Schuster R, Ertl G. Physical Review Letters 2004;92
36. Hayazawa N, Tarun A, Inouye Y, Kawata S. Journal of Applied Physics 2002;92:6983–6986.
37. Novotny L, Sanchez EJ, Sunney Xie X. Ultramicroscopy 1998;71:21–29.
38. Hayazawa N, Saito Y, Kawata S. Applied Physics Letters 2004;85:6239–6241.
39. Steidtner J, Pettinger B. Review of Scientific Instruments 2007;78
40. Youngworth KS, Brown TG. Optics Express 2000;7:77–87. [PubMed: 19404372]
41. Saito Y, K M, Hiraga D, Fujita K, Kawano S, Smith NI, Inouye Y, Kawata S. Journal of Raman Spectroscopy 2008;39:1643–1648.
42. Sun WX, Shen ZX. Ultramicroscopy 2003;94:237–244. [PubMed: 12524194]
43. Sun WX, Shen ZX. Journal of Raman Spectroscopy 2003;34:668–676.
44. Schultz ZD, Stranick SJ, Levin IW. Applied Spectroscopy 2008;62:1173–1179. [PubMed: 19007457]
45. Tong LM, Li ZP, Zhu T, Xu HX, Liu ZF. Journal of Physical Chemistry C 2008;112:7119–7123.
46. Olk P, Renger J, Hartling T, Wenzel MT, Eng LM. Nano Letters 2007;7:1736–1740. [PubMed: 17497823]
47. Xu HX, Kall M. Chemphyschem 2003;4:1001–1005. [PubMed: 14562448]
48. Graupner R. Journal of Raman Spectroscopy 2007;38:673–683.

49. Kitagawa, T.; Hirota, S. Handbook of Vibrational Spectroscopy. Griffiths, PR., editor. Vol. 5. John Wiley & Sons Ltd; Chichester: 2002. p. 3426-3446.

50. Betzig E, Patterson GH, Sougrat R, Lindwasser OW, Olenych S, Bonifacino JS, Davidson MW, Lippincott-Schwartz J, Hess HF. Science 2006;313:1642–1645. [PubMed: 16902090]

51. Rust MJ, Bates M, Zhuang XW. Nature Methods 2006;3:793–795. [PubMed: 16896339]

52. Bailo E, Deckert V. Angewandte Chemie International Edition 2008;47:1658–1661.

53. Fernandez DC, Bhargava R, Hewitt SM, Levin IW. Nature Biotechnology 2005;23:469–474.

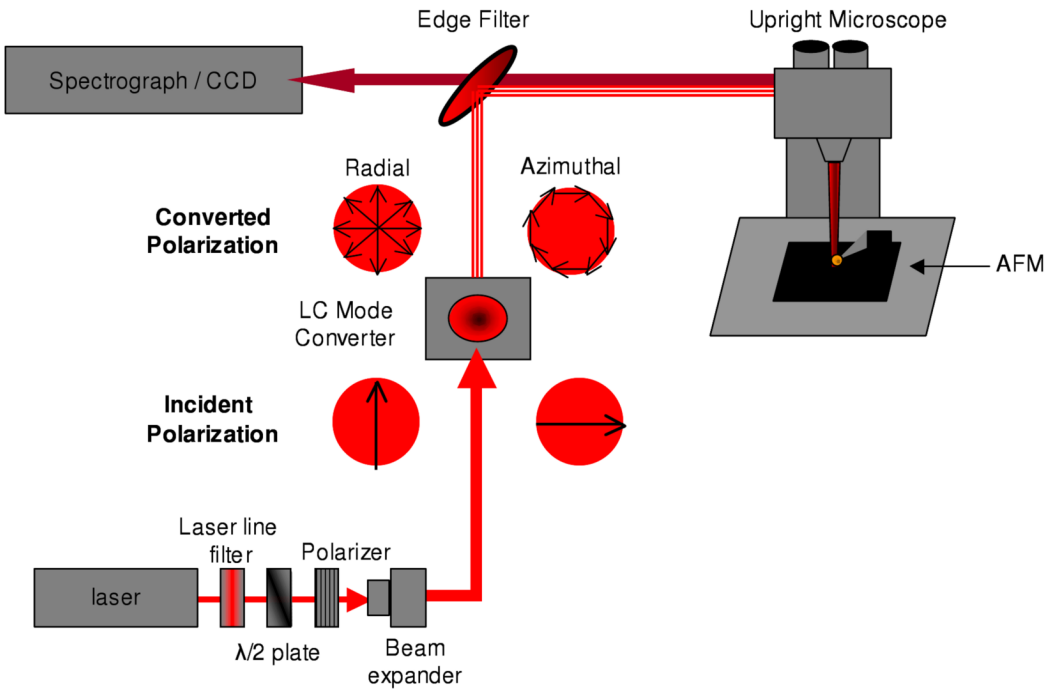

Figure 1.

The schematic illustrates the polarization conversion used in our TERS microscope. A 647 nm laser is linearly polarized in the vertical direction. The beam is expanded and passes through a liquid crystal model converter. The output from the mode converter can be switched from radial polarization (left) to an azimuthal polarization (right) by alternating from vertical to horizontal polarization. The converted polarization is then passed through an upright microscope and focused by means of a 100×, NA=0.70, objective, onto a nanoparticle AFM tip. The Raman scattering is collected and spectrally resolved using a spectrograph and CCD camera.

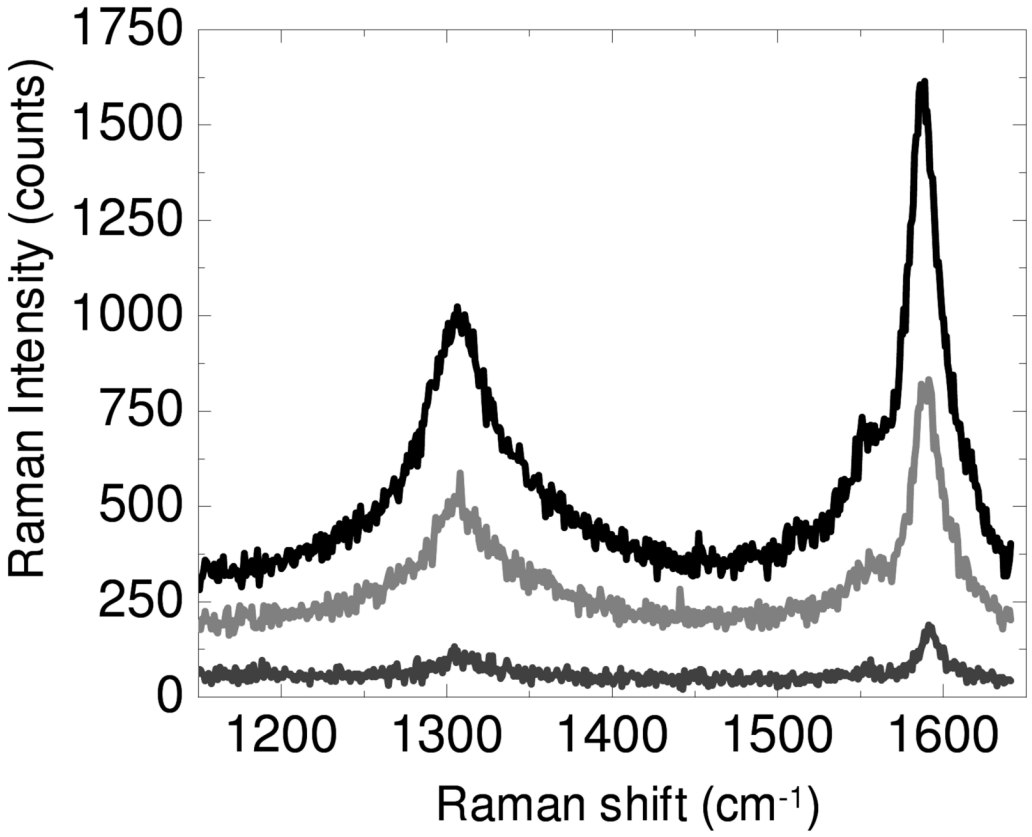

Figure 2.
Raman spectra are shown from a carbon nanotube sample where radial polarized (black) and azimuthal polarized (light grey) light is focused onto the nanoparticle tip. The far field spectrum (dark grey), nearly identical in either polarization, obtained with the AFM tip retracted from the surface is significantly diminished.

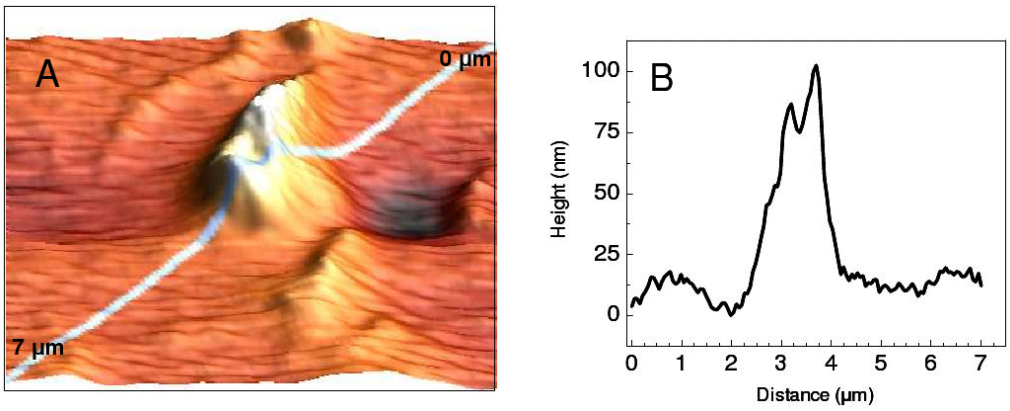

Figure 3.
A 5 µm × 5 µm AFM image of single wall carbon nanotubes is depicted in A. The topographic profile obtained from the top right corner to the bottom left corner is shown in B.

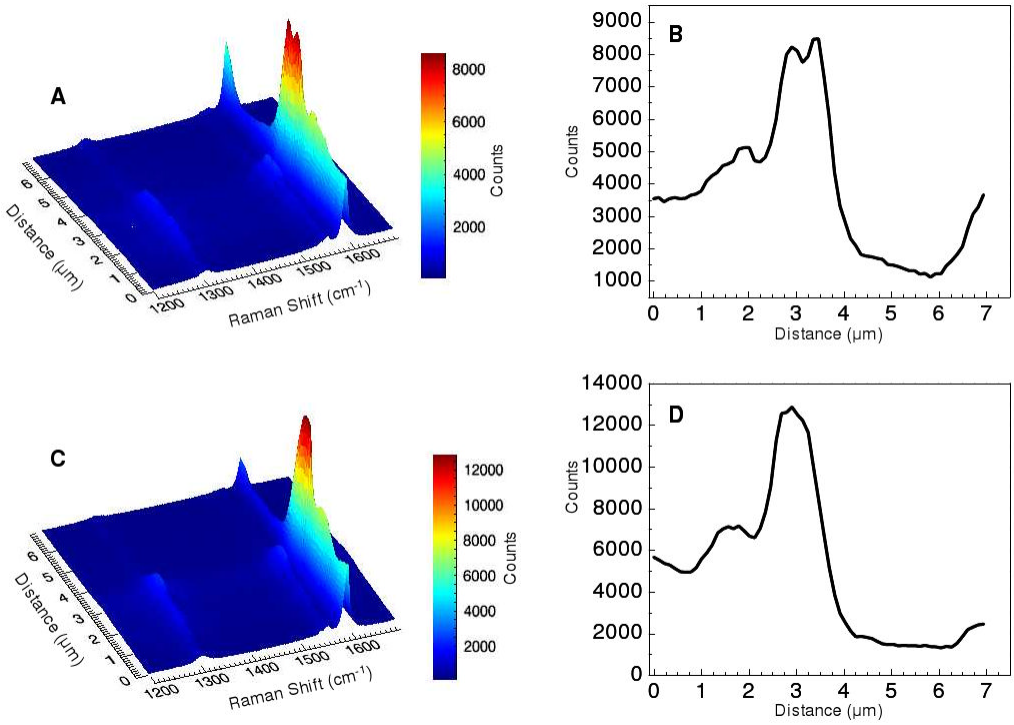

Figure 4.

The TERS spectra obtained using radial polarization along the diagonal profile shown in figure 3B are plotted distance vs. Raman shift in panel A. The radial polarization Raman intensity profile observed at 1590 cm^{-1}, is shown in B. Panel C shows the distance vs. Raman shift plot obtained using azimuthal polarization along the same region. The azimuthal polarization Raman intensity profile at 1590 cm^{-1} is shown in D.

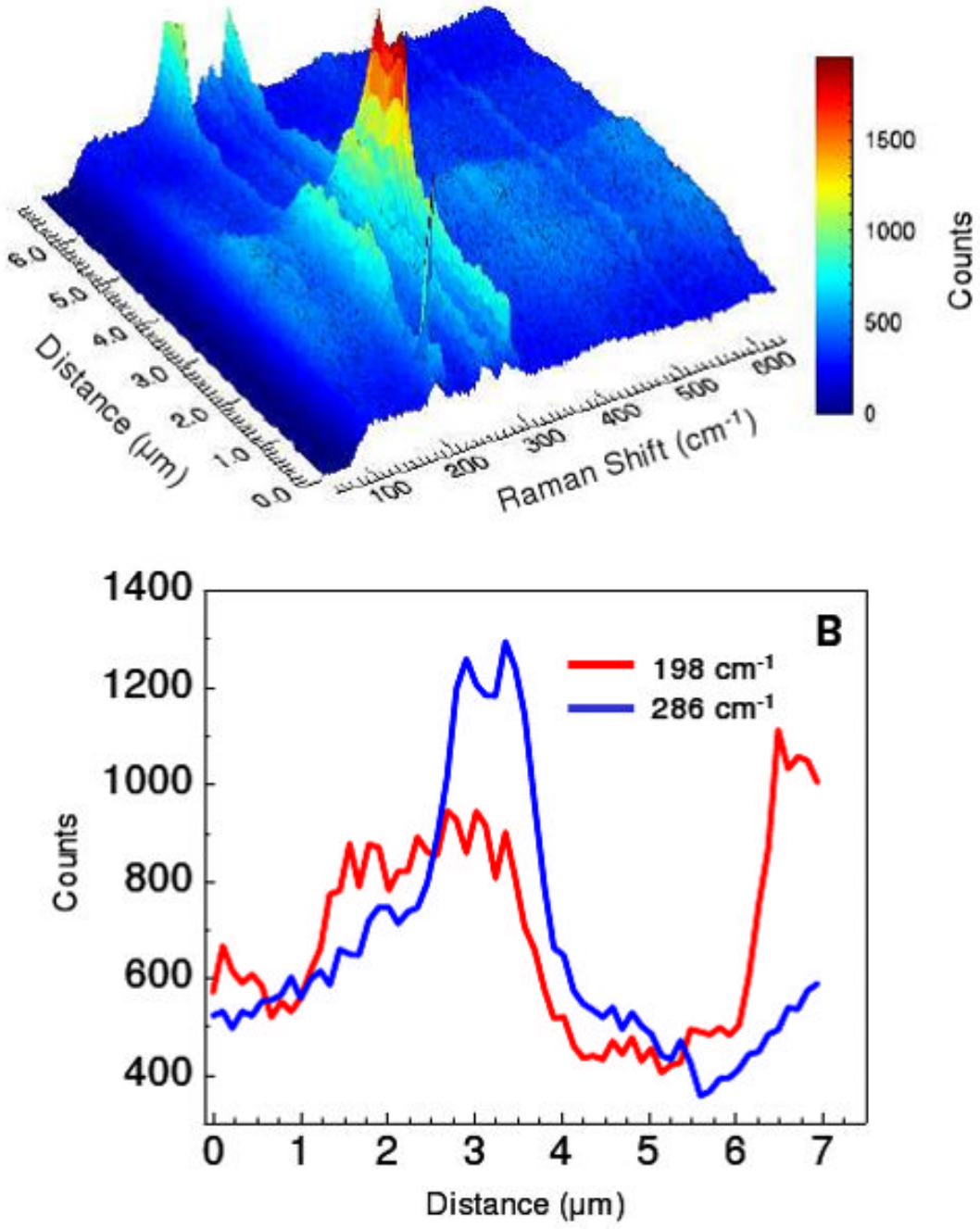

Figure 5.

The radial polarized Raman spectrum, observed in the frequency region corresponding to the radial breathing modes of carbon nanotubes and probed along the diagonal profile in figure 3B, is plotted in A. The Raman intensity profiles at 198 and 286 cm^{-1}, corresponding to 12 and 8 Å nanotubes respectively, shown in B illustrate the spatial heterogeneity of the nanotubes.

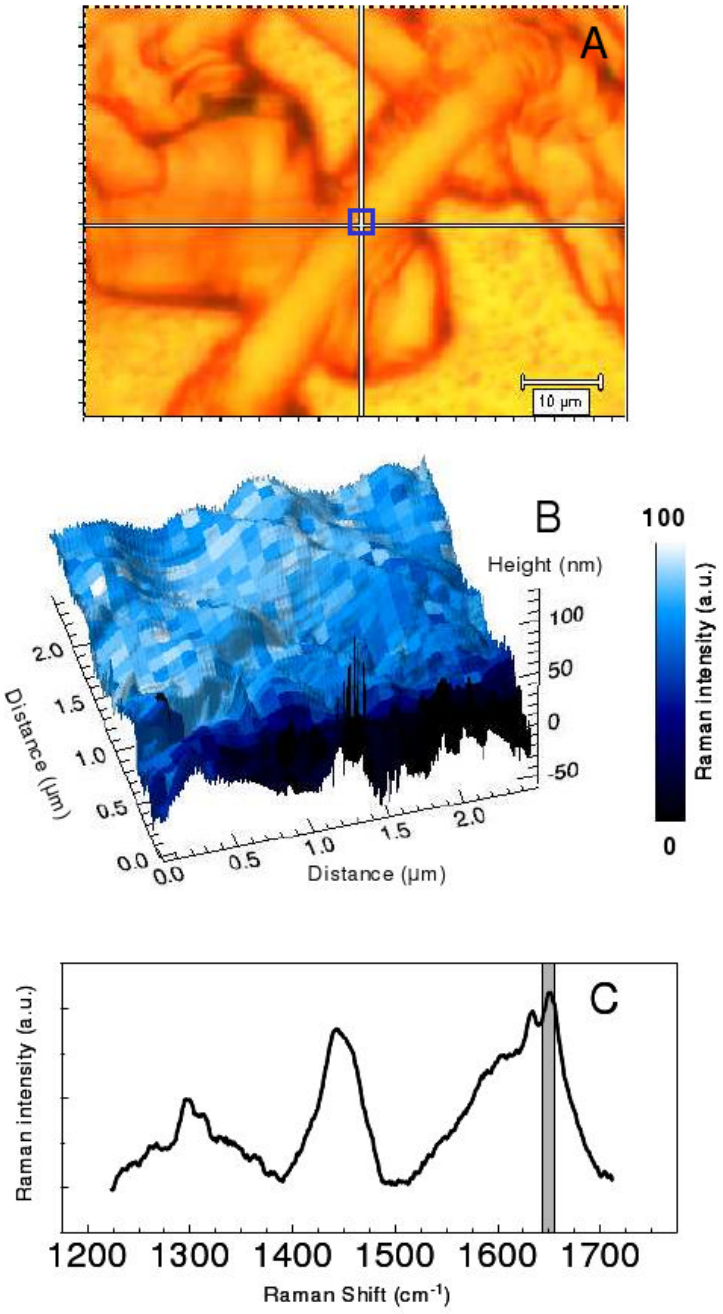

Figure 6.

The visible image of a rod photoreceptor cell is shown in A. The 2.5 μm × 2.5 μm blue box in A corresponds to the combined AFM topography – Raman Intensity plot (B). In B the baseline corrected intensity of the 1655 cm^{-1} band (C, grey box) is shown to vary on the size of the map pixels, 97 nm.